Internal Note 11/2010

Signal behaviour in fibre detectors at MAMI

P. Achenbach, A. Esser, P. Žugec
Institut für Kernphysik, Johannes Gutenberg Universität Mainz, Germany
DATED: 30 November 2010

Light attenuation in Scintillating Fibres

In order to precisely determine the attenuation parameters of standard (Non-S) type SCSF-78 fibres from Kuraray, the experimental setup shown in Fig. 1 was employed. It consisted of a L = 10 m long fibre, with both ends glued to a plastic connector and coupled with the R7259K Hamamatsu Photonics multi-anode photomultiplier, supplied with 900 V HV. The fibre was bent in circles and put inside a black container for protection from surrounding light sources. The fibre itself was Ø = 0.83 mm in diameter, with a cladding thickness of 0.05 mm, making the active core Ø = 0.73 mm wide. The refractive index of the polystyrene (PS) core is n_{core} = 1.59, while that of the inner polymethylmethacrylate (PMMA) cladding is n_{in} = 1.49, and of the outer fluorinated polymer (FP) cladding n_{out} = 1.42. The spectral maximum of this blue light emitting fibre is reached at 440 nm. A fast (200 ps pulse duration) ultraviolet laser was used as light source, with a pulse repetition frequency of 800 Hz. For the photomultiplier signals a conventional electronic readout system with ADC was employed.

The laser hit-position x was shifted along the length of the fibre by manually moving the fibre in respect to the immobile laser, while their coupling was performed by adjusting and taping the fibre over the beam. In course of every measurement the ADC counts (ADC1, ADC2) from every edge of the fibre and their ratio R were monitored. As a result of the numerical aperture of the outgoing scintillation light at the fibre ends the channels that are neighbouring the central one also registered part of the light pulse. Accordingly, for the overall ADC count contributions from closest neighbouring channels were included.

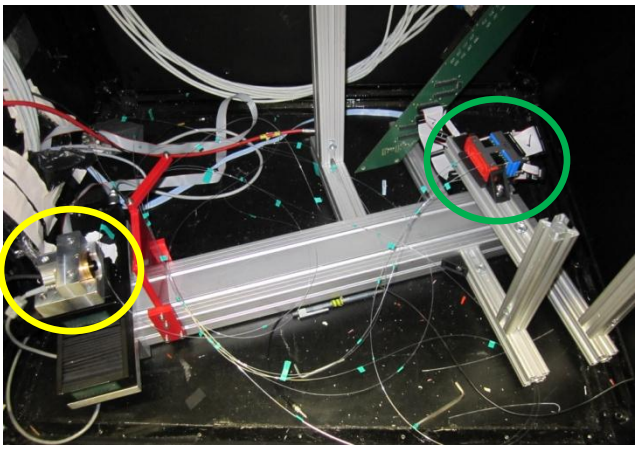

Figure 1: Experimental setup consisting of SCSF-78 Kuraray fibre coupled to R7259 Hamamatsu Photonics photomultiplier (green circle). Light pulses were induced by a fast ultraviolet laser (yellow circle).

Measured mean values from basically Gaussian ADC distributions from both ends of the fibre for 44 different laser hit-points are shown in Fig. 2. Since the registered ADC counts are highly sensitive to the centering of the fibre over the laser beam, strong fluctuations were experienced. However, the trend of ADC counts rising with the laser approaching the corresponding end of the fibre is clearly visible.

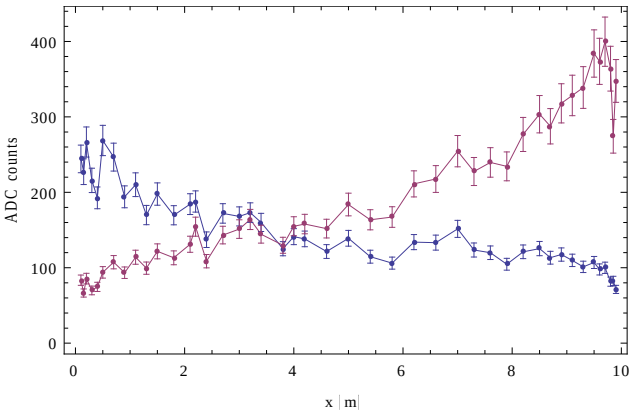

Figure 2: Mean ADC counts from both ends of the scintillating fibre for different positions of the laser hit-point along the fibre.

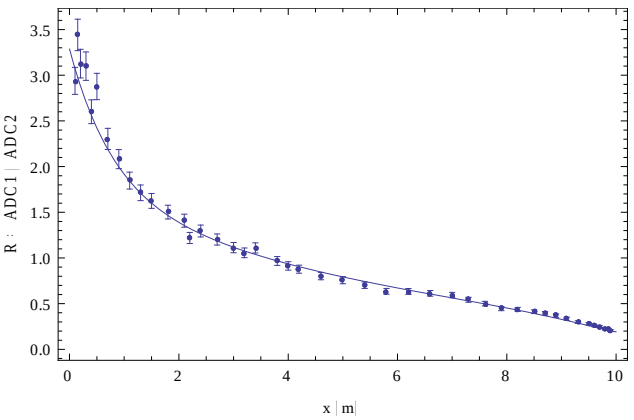

Figure 3: Measured ratios of ADC-counts from the two ends of the fibre. Full line shows the result of fitting to the predefined model.

ADC count ratios are shown in Fig. 3. Assuming a two-component attenuation of light inside the fibre, with A_i as expected ADC counts from non-attenuated pulse at i-th fibre end, λ_1, λ_2 as attenuation lengths and f as fraction of the first component:

$$\mathrm{ADC}_i\ \ x\ = A_i\left[\ f e^{-x/\lambda_1}\ +\ 1-f\ \ e^{-x/\lambda_2}\ \right]$$

the ratio R is defined as:

$$R=\frac{ADC_1\ \ x}{ADC_2\ \ L-x}=\alpha\frac{f e^{-x/\lambda_1}\ +\ 1-f\ \ e^{-x/\lambda_2}}{f e^{-\ L-x\ /\lambda_1}\ +\ 1-f\ \ e^{-\ L-x\ /\lambda_2}}$$

which is, with $\alpha = A_1/A_2$, the model used for fitting the experimental data shown in Fig. 3. Results for model's parameters obtained by fitting with experimental error taken into account are:

$$\alpha = \ 0.793 \pm 0.006$$

$$f = \ 0.53 \pm 0.03$$

$$\lambda_1 = \ 13 \pm 1 \ \ \mathrm{m}$$

$$\lambda_2 = \ 0.8 \pm 0.2 \ \ \mathrm{m}$$

While the longer attenuation length is due to absorption of light inside the scintillating core, the shorter one is attributed to losses inside the cladding and increased absorption of shorter wavelengths light. After calculating χ^2 value of χ^2 = 57.6 for the fitting model, with 40 as the number of degrees of freedom, we can conclude that the reliability of both model and the obtained results is satisfactory.

As a measure of control over the consistency of the results, we have also fitted the measured points from Fig. 2 to the previously proposed two-component exponential form for the ADC counts. Assuming mutual parameters f, λ_1, λ_2 for both curves and considering increased variance of their values:

$$f = \ 0.6 \pm 0.4$$

$$\lambda_1 = \ 14 \pm 11 \ \ \mathrm{m}$$

$$\lambda_2 = \ 2 \pm 2 \ \ \mathrm{m}$$

the obtained results do not differ much from those determined by the ADC count ratio dependency, despite strong fluctuations in trends from Fig. 2. Naturally, because of excessive variances as a direct consequence of such fluctuations and strongly increased χ^2 values of χ_1^2 = 193.2 for blue points from Figure 2 and χ_2^2 = 293.4 for purple ones, the initially determined values are considered to be more reliable.

Signal discrimination

Signal discrimination in experiments using the fibre detectors for the Kaos spectrometer are performed using double-threshold discriminator boards, each containing eight GSI-Chip3 chips. A systematic examination of these discriminators was performed. For purposes of providing input signals we have employed the earlier experimental setup consisting of a fast ultraviolet

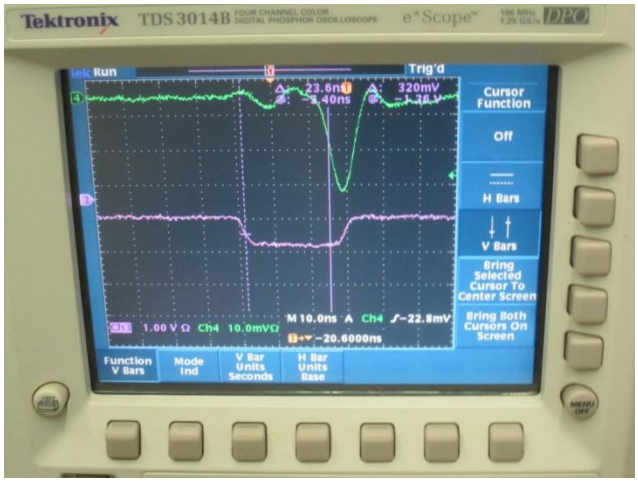

Figure 4: An example of the Tektronix TDS 3014B digital oscilloscope readout. The input signal from the photomultiplier is shown in green (5 mV/ns rising edge slope; 6 ns rise time), the output signal from the discriminator in purple. Because of coaxial cable delays, the output signal precedes the input signal.

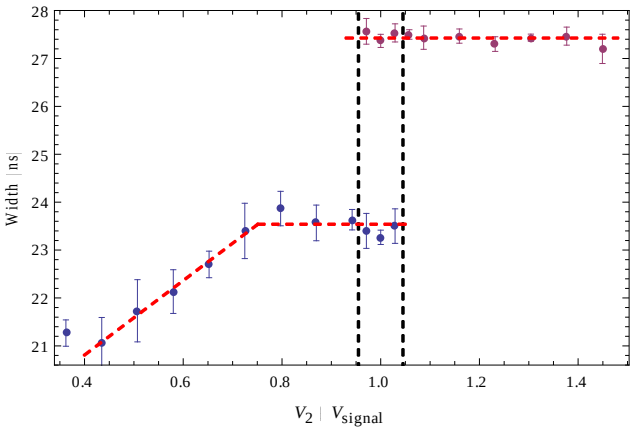

Figure 5: Output signal width depending on the ratio of the upper threshold voltage and the input signal amplitude. Blue points define a regime of signal crossing both thresholds, while purple ones regime of only lower threshold crossed. The transitional area is isolated by black dashed lines, while red dashed lines follow the local trend serving as a guide for an eye.

laser, a scintillating fibre and a multichannel photomultiplier (Fig. 1). For signal readout, both input and output, a Tektronix TDS 3014B four-channel digital oscilloscope was used. An example of input and output signals is shown in Fig. 4.

Instead of varying the amplitude of the input signal in respect to fixed discriminator thresholds, we have selected to vary the thresholds in respect to a well defined amplitude. Threshold control is performed via computer interface enabling changes in steps of 1 inside a range of 0-2040. Lower and upper threshold reference voltages, V_1 and V_2, respectively, were varied keeping a constant ratio of :

$$V_2/V_1 = 3/2$$

The input signal from Figure 4 shows the secondary voltage peaks along a central one. Because of that occurrence the value for lower trigger was set above this voltage range during all measurements, enabling consistent triggering generated only by the rising edge of highest peak.

The results of measuring the output signals' delay and width are shown in Figs. 5-7. The width measurements in Fig. 5 show the two regimes for the discriminator functionality – one in case the upper threshold is crossed (blue points) and the other in case it is not (purple points). Because of input signal fluctuations, when the upper threshold approaches the signal amplitude, occurrences of crossing and its absence start to combine, resulting in a transitional voltage region where both regimes are present. While the lower threshold voltage V_1 can be calibrated in reference to parameter x_1 simply by varying it around the known input signal amplitude and observing the output signal appearance and/or disappearance, calibration procedure for upper threshold can be performed by closely examining the transition between the two regimes.

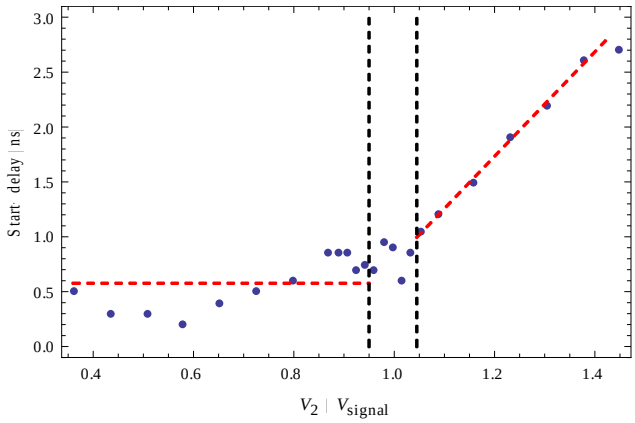

Figure 6: Measured delays for the output signal appearance in relation to a fixed point (maximum) of the input signal. Black dashed lines separate the transitional area between the two regimes depending on the input signal crossing the upper threshold. Red lines are a guide to the eyes, following the local trend.

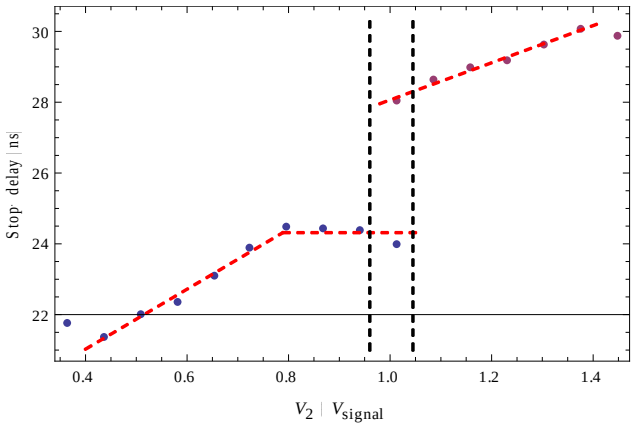

Figure 7: Output signal trailing edge delay in reference to the input signal maximum, obtained by summing results from Figure 5 and 6. The practice of colouring points and using dashed lines is identical to that from Figure 5.

Fig. 6 presents measurements of the output signal's delay in relation to a fixed input signal's point, for which its maximum was selected. The presence of two different regimes for delay can be explained by separate triggering mechanisms depending on whether an upper threshold was crossed or not.

Fig. 7 shows the dependence for moment of output signal's trailing edge, constructed as a sum of measured delays from Fig. 6 and widths from Fig. 5, for comparison with those values.

Timing properties of a signal

For investigation of timing properties of a signal from the fibre detector – specifically, distribution of time differences for signals' arrival at opposite ends of the fibre, the "resolutional distribution" we have employed experimental setup from Fig. 8. The central part of this setup consists of a Saint-Gobain wavelength shifting fibre BCF-92, firmly attached in place and coupled with Hamamatsu multi-pixel photon counter (silicon photomultiplier, SiPM) S10362-11-050U (metal type) via optical grease. Fibre is fast blue-to-green light shifting type, L = 121.2 cm in length, with a square cross section of 1×1 mm^2 matching the SiPM active area of 400 pixels. Both SiPMs were selected for the same value of a working voltage, which was set to 71.5 V. Again, a fast ultraviolet laser was used as a source for light pulses. For signal amplification a single-stage amplifier with THS3201 chip was selected. For signal readout analogue electronic system was used, combining ADC, TDC, coincidence units with simple leading edge discriminator.

Identically to the procedure with 10 m long SCSF-78 fibre, we have used measured values for ADC counts and their ratios to examine light attenuation properties of a BCF-92 fibre. Measured results for 19 equidistant positions of a laser along the fibre are shown in Figures 9 & 10. Almost constant trend from Fig. 9 for ADC counts at one end of the fibre (blue points) is a result of a slight increase in laser temperature and consequent rise in light output intensity, shifting ADC spectrum to values higher than expected for a given laser position. By allowing laser to cool down just enough for signal amplitude not to cause ADC saturation, counts from one end of the fibre were kept basically constant, making them inconsistent and unreliable for extrapolation of light attenuation properties. Still, ADC count ratios from Figure 10, corrected for voltage and ADC offset, show stable trend of expected form. After initial examination, it was concluded that a single component description by

$$R = \alpha e^{L-2x/\lambda}$$

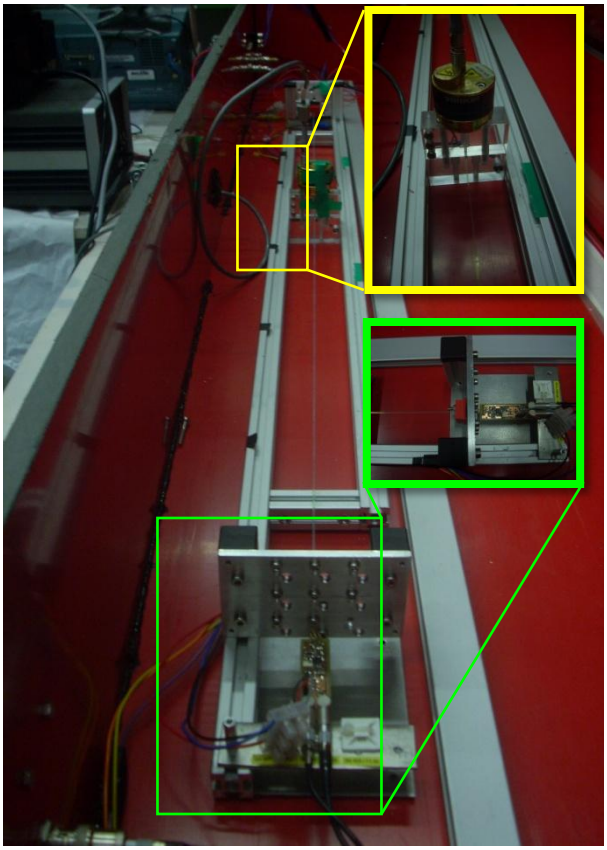

Figure 8: Experimental setup for investigation of BCF-92 Saint-Gobain wavelength shifting fibre with Hamamatsu S10362-11-050U silicon photomultiplier (metal type). Green inserted frame shows construction of fibre-SiPM-amplifier coupling, with single-stage amplifier incorporating THS3201 chip. Yellow frame shows the fixation of the laser over the fibre.

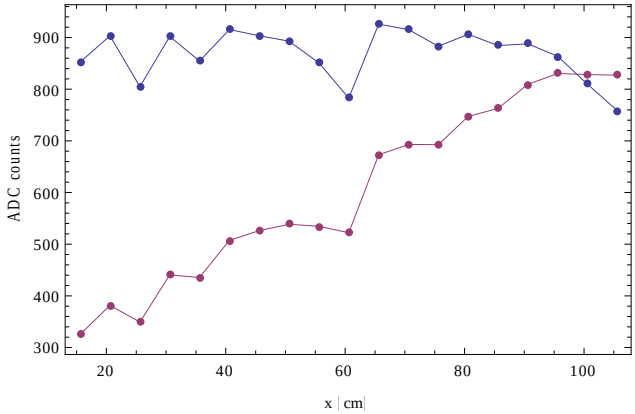

Figure 9: ADC counts from opposite ends of the BCF-92 fibre (denoted by different colour), for light pulses induced by a fast ultraviolet laser at different positions along the fibre. The light intensity increased because of heating during the measurements.

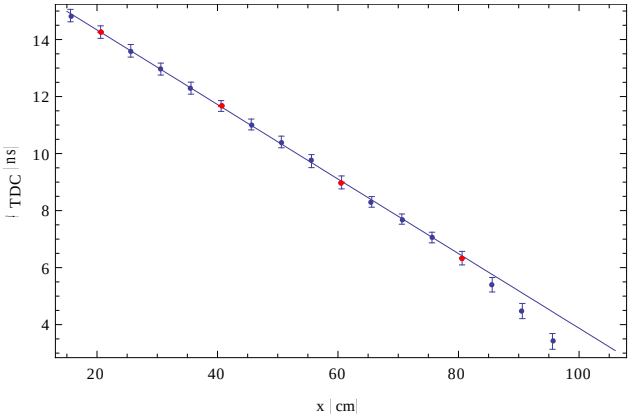

Figure 10: ADC counts ratio dependency (pedestal corrected) on laser position along the fibre. Full line shows result of fitting to the single-component exponential form, with obtained value of λ = 249 cm for attenuation length. Red points have been assigned an experimental error.

is the best fit for the given points. The obtained parameter values are:

$$\alpha = \ 1.187 \pm 0.003$$

$$\lambda = \ 249 \pm 3 \ \ \text{cm}$$

Fig. 11 presents measured results for a mean value μ_{TDC} of a resolutional distribution, that is central value for difference of light pulses' arrival times at opposite ends of the fibre. Average full width of half maximum (FWHM) of measured distributions is:

$$\text{FWHM} = \ 0.44 \pm 0.06 \ \ \text{ns}$$

For the initial 13 of a total of 19 measured points significantly improved linearity was observed. Therefore, these alone were taken into account for fitting to the linear model:

$$\mu_{TDC} = ax + b$$

leading to a value for parameter a of:

$$a = \ -0.1307 \pm 0.0007 \ \ \text{ns}\,\text{cm}^{-1}$$

Free parameter b is of reduced physical importance since it incorporates the difference of coaxial cables' delay during signal transmission – value entirely unrelated to fibre itself. However, after expressing μ_{TDC} in terms of physical parameters:

$$\mu_{TDC} = \frac{L - 2x}{v_{eff}} + \Delta T$$

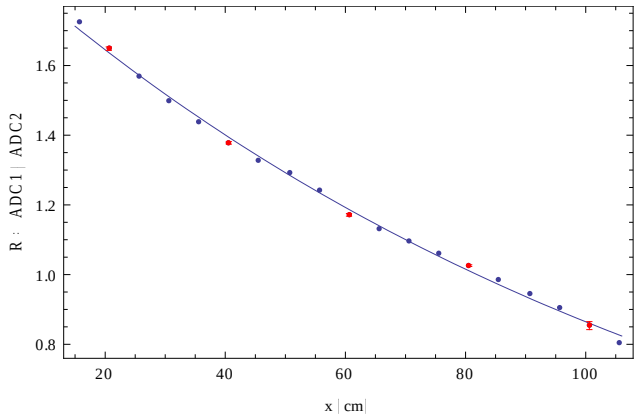

Figure 11: Resolutional distribution mean measurements with experimental error assigned to the red points. Variances for blue points are given by FWHM of measured distributions. Full line shows a result of a linear fit applied to initial 13 points.

with v_{eff} as an effective light propagation speed in the fibre and coaxial cables' delay difference ΔT, we can directly see the physical interpretation for slope a:

$$a = -\frac{2}{v_{eff}}$$

providing us with estimation for v_{eff}:

$$v_{eff} = 15.30 \pm 0.08 \ \ \mathrm{cm\,ns^{-1}}$$

We are developing simple model to describe physical origin of v_{eff}. Assuming photon emission at an axial angle θ_1 toward one end of the fibre and at θ_2 toward the opposite end, difference of arrival times is given by:

$$\mu_{TDC}\ \ x;\theta_1,\theta_2\ \ = \frac{n_{core}}{c}\left(\frac{L-x}{\cos\theta_1} - \frac{x}{\cos\theta_2}\right) + \Delta T$$

with speed of light c (in vacuum) and n_{core} = 1.60 as refractive index of the fibre core. Averaging this difference under assumption of isotropic spatial distribution $dp(\theta)$ of emitted photons, normalized for angles up to critical angle θ_C for total reflection, given by $\cos\theta_C = n_{clad} / n_{core}$:

$$dp\ \ \theta\ \ = -\frac{n_{clad}}{n_{clad}-n_{core}} d\ \ \cos\theta$$

with n_{clad} = 1.49 as refractive index of the fibre cladding, after integration:

$$\mu_{TDC}\ \ x\ \ = \int_0^{\theta_C}\int_0^{\theta_C} \mu_{TDC}\ \ x;\theta_1,\theta_2\ \ dp\ \ \theta_1\ \ dp\ \ \theta_2$$

we are left with final expression for fitting model:

$$\mu_{TDC} = \frac{L-2x}{c}\frac{n_{core}^2}{n_{core}-n_{clad}}\ln\frac{n_{core}}{n_{clad}} + \Delta T$$

and, consequently, for v_{eff}:

$$v_{eff} = \frac{n_{core}-n_{clad}}{n_{core}^2 \ln\ n_{core}/n_{clad}} c$$

Entering known values into previous expression yields the result of v_{eff} = 18.10 cm ns^{-1}. However, considering even simpler model that includes only the most probable angle θ_C for photons arriving to the ends of the fibre:

$$\mu_{TDC}\ \ x\ \ = \frac{n_{core}}{c}\frac{L-2x}{\cos\theta_C} + \Delta T$$

with corresponding effective speed:

$$v_{eff} = \frac{n_{clad}}{n_{core}^2} c$$

we are left with v_{eff} = 17.46 cm ns^{-1}, result that is in better agreement with experimentally obtained value.